Supplementary information

Memoli, Fury *et al.*, "Acoustic force measurements on polymer-coated microbubbles in a microfluidic device", J. Acoust. Soc. Am. (2017)

I. SCHEMATIC OF THE MEASUREMENT PROCEDURES USED IN THIS WORK

Three different methods for characterising an acoustofluidic device have been used in this work, each of them resulting in a different experimental set-up. Figure 1 reports a schematic description of the methods discussed in this work, highlighting the different phases of the process leading from input data to local pressure measurements and the experimental set-up utilised. In particular, each flow chart highlights (with dotted lines) the hypotheses behind each method. Figure 1 shows that:

- the laser vibrometer has the simplest experimental apparatus, while the optical tweezers have the more complex one;
- bubble/particle tracking has the highest number of hypotheses to be verified for it to be accurate;
- FE-calibrated laser vibrometry and particle/bubble tracking rely on the hypothesis of a standing wave in the microchannel, which instead is one of the outputs of the optical tweezers method. In this sense, used simultaneously, the three methods are complementary.

II. DETAILED DESCRIPTION OF THE MICROFLUIDIC CHIP

Figure 2 presents a technical drawing of the microfluidic chip discussed in this work. The chip was designed at the National Physical Laboratory (NPL) and manufactured by Dolomite, who fused together 4 differently etched glass surfaces. Also highlighted are the relative positions of the Nanoport^{TM} fittings, the piezo transducer, the illumintion window and the Nikon objective used for the optical tweezers. The central area of the K-shaped manifold, where simultaneous trapping was investigated, covered the main channel in the X direction between 12.11 mm and 12.89 mm.

III. DESCRIPTION OF THE HOFF MODEL[1]

According to the Hoff model, tthe resonance frequency of a coated microbubble is given by[1,2]:

$$f_s = \frac{1}{2\pi R_0}\sqrt{\frac{1}{\rho_L}\left[3\gamma P_0 + \frac{2(3\gamma-1)\sigma}{R_0} + \frac{4\chi}{R_0}\right]} \quad (1)$$

where R_0 is the equilibrium radius of the bubble, ρ_l is the liquid density, γ is the ratio of the specific heats of the gas inside the bubble, P_0 is the hydrostatic pressure, σ is the surface tension at the gas-liquid interface, and χ is the elasticity parameter of the shell.

IV. SIZE DISTRIBUTIONS

Figure 3 reports the size distributions for CPC4000 and Expancel WU-20, as determined by optical microscopy in this study. The two distributions account respectively for 100 particles and 300 bubbles, all of them tracked during pressure measurements. For the purposes of this paper, it was deemed sufficient to compare the key statistical parameters found optically with those reported by the manufacturer (available for CPC4000 particles). Since an excellent agreement (within the uncertainties), the same method was used for the bubbles (for which the size distribution is unknown).

V. DRAG, INERTIAL FORCES, TEMPERATURE EFFECTS

According to Faez et al.[3], many models based on force-balance describe bubble dynamics using Stokes' drag in the form $F_{\mathrm{drag}} = 6\pi a \mu_{\mathrm{l}} v_{\mathrm{p}}$ where a is the bubble radius, μ_{l} is the viscosity of the liquid and v_{p} is the bubble velocity. This is a formula valid strictly only for solid particles, but Celata et al.[4] confirm that this formula is valid also for bubbles rising in surfactant-water solutions, when the Reynolds number is smaller than 0.1: a condition that was always met in our experiments.
Rabaud et al.[5] show however that it is necessary to correct the drag force for confined bubbles whose surface is always in contact with the wall of a microfluidic system, using a power of $\xi = (a/L)$, where L is the size of the microchannel. The additive correction proposed by Rabaud et al. for $\xi > 0.6$ is proportional to $\xi^{1/5}$. A more complex expression for the increased drag can be found in the classical text by Clift et al.[6], who for low Reynolds numbers and $\xi < 0.5$ propose as leading term ξ^5. Under similar conditions, Barnkob et al.[7] proposes

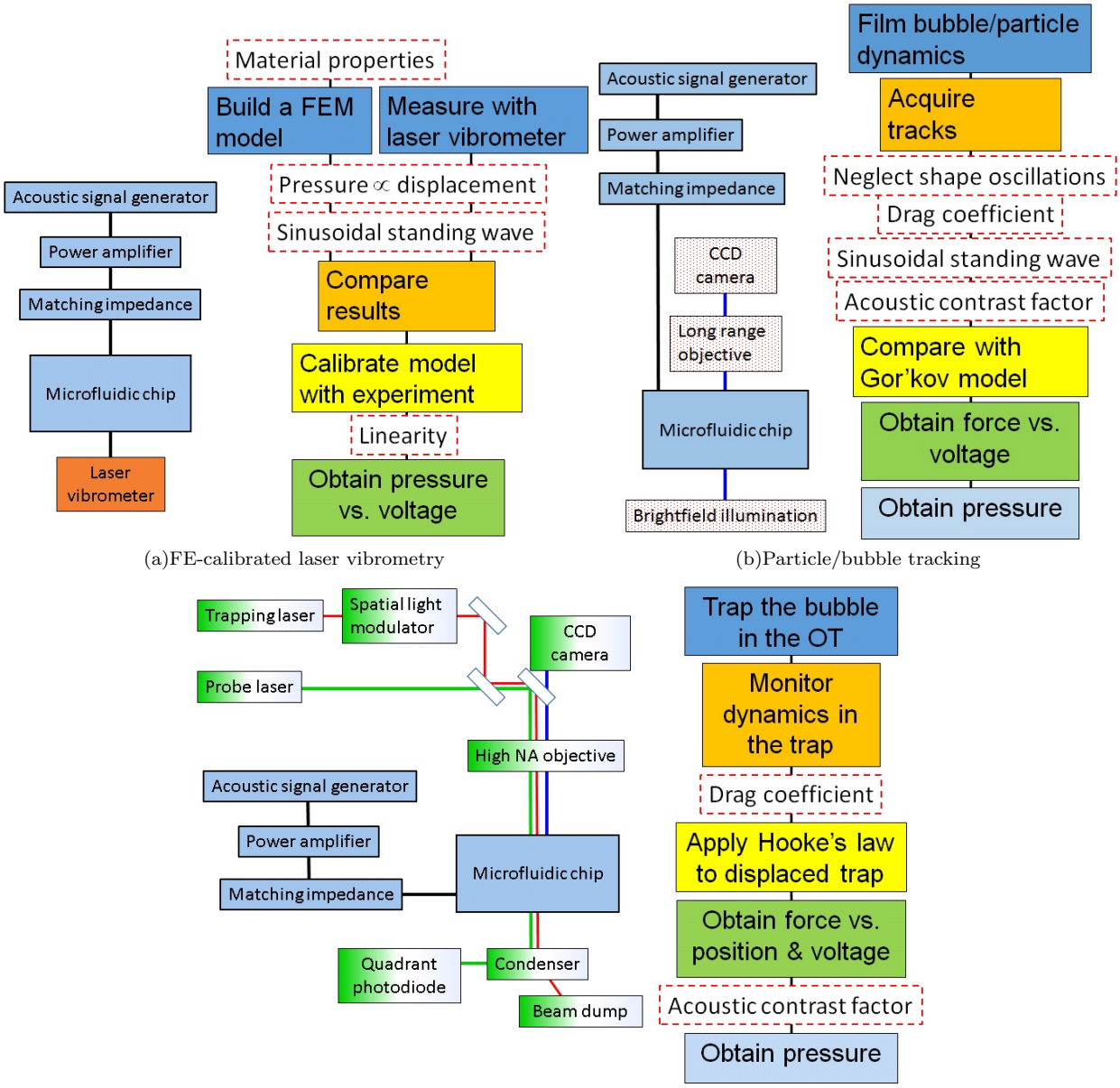

(a)FE-calibrated laser vibrometry

(b)Particle/bubble tracking

(c)Calibrated optical tweezers

FIG. 1. A schematic descriptions of the measurement methods used in this study. Each sketch reports the main parts of the experimental set-up and a flow chart representing the different steps leading from measurements to a pressure value. Each flow chart highlights (dotted lines) the hypotheses needed in the particular method.

a leading correction $\sim \xi^2$. The particular case of the interaction of bubbles with the walls of an acoustically resonant pipe has been explored by T. G. Leighton[8], who shows an effect on the inertia and a different damping for bubbles moving, resulting in a change in their resonant frequency.

In the experiments presented here, the cumulative correction to drag due to the all the effects above - for the range of diameters considered - was estimated to be below 0.5% and was therefore neglected.

VI. DETAILED RESULTS OF AN IMPEDANCE SCAN

Figure 4 reports the real part of a typical impedance scan for microchip "C", measured across the terminations of the electrical matching circuit. Particularly interesting are the frequencies where the measured impedance corresponds to the 50 Ω, where energy tranfer to the chip is maximised, and the ones which present a peak. The position of the peaks offered the first estimate of where trapping might occur[9].

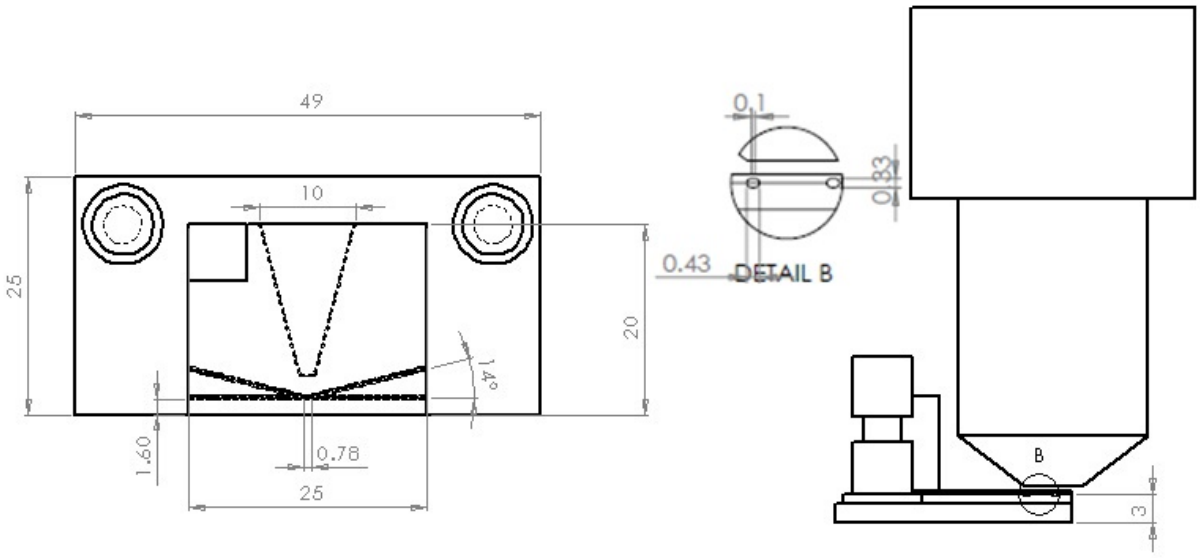

FIG. 2. This figure reports a detailed drawing of the microfluidic chip, as shown in figure 1 of the main paper. Also highlighted are the Nanoport^{TM} fittings, the illumination window, the piezo transducer, the Nikon objective used for the optical tweezers and a detailed section of the microchannels. In particular, the section is formed (from left to right) by a semi-circular region (diameter 0.33 mm), a rectangle 0.1 mm wide and 0.33 mm high, another semi-circular region (diameter 0.33 mm).

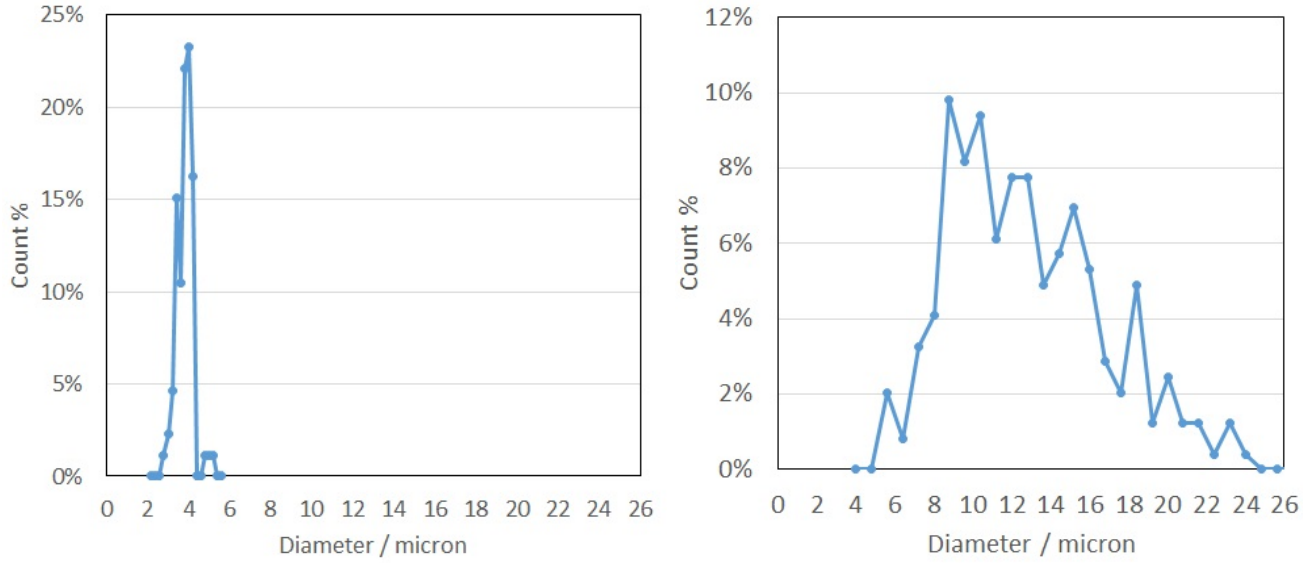

(a)CPC4000 (b)Expancel

FIG. 3. Size distributions of the prticles and bubbles used in this work, as determined by optical microscopy. Calibration was obtained using a NPL graticule.

VII. CONVERGENCE ANALYSIS FOR PRESSURE SIMULATIONS

Figure 5 reports the acoustic pressure magnitude inside the microchannel for increasingly refined meshes at 160 kHz. The numbers in the legend correspond to the average element dimension in a given mesh. The results in the main text correspond to the cyan curve (i.e. a mean element size of 0.67 mm). In conclusion, the mesh analysis does converge as the element size decreases. The choice of a mean element size of 0.67 mm, relative to the data presented in the main text, was a compromise be-

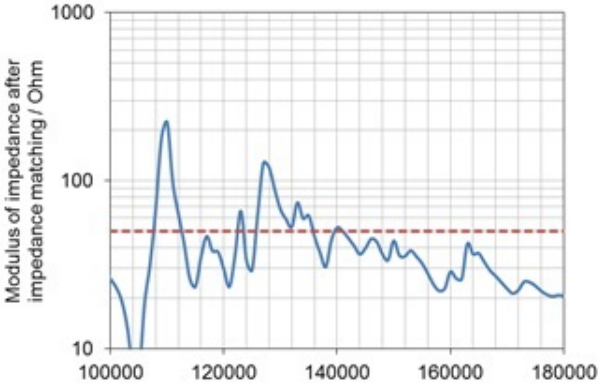

FIG. 4. Impedance spectrum, measured before the impedance matching circuit. The output impedance of the E&I amplifier (50 Ω) is highlighted by a dashed line.

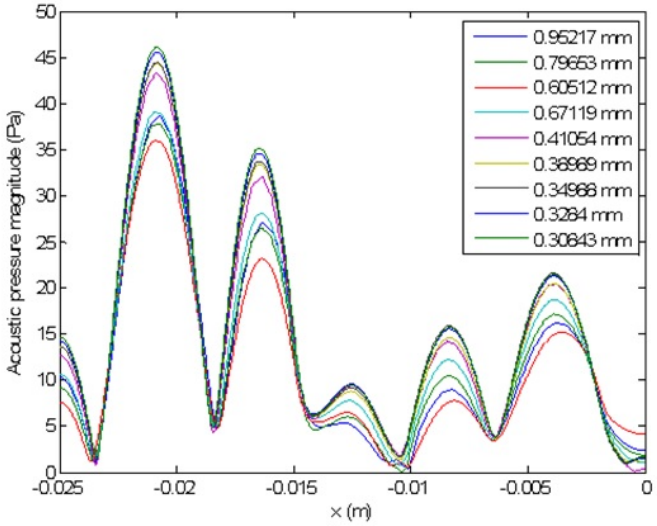

FIG. 5. Pressure magnitude inside the microchannel for increasingly refined meshes at 160 kHz.

tween retaining sufficient features of the converged solution whilst having acceptable run times.

[1]Lars Hoff, Per C. Sontum, and Jens M. Hovem. Oscillations of polymeric microbubbles: Effect of the encapsulating shell. *The Journal of the Acoustical Society of America*, 107(4):2272–2280, 2000.

[2]Y. Gong, M. Cabodi, and T. Porter. Pressure-dependent resonance frequency for lipid-coated microbubbles at low acoustic pressures. In *IEEE International Ultrasonics Symposium Proceedings*, pages 1932–1935, 2010.

[3]T. Faez, M. Emmer, K. Kooiman, M. Versluis, A. F. W. van der Steen, and N. de Jong. 20 years of ultrasound contrast agent modeling. *IEEE Transactions on Ultrasonics, Ferroelectrics, and Frequency Control*, 60(1), January 2013.

[4]Gian Piero Celata, Francesco DAnnibale, Paolo Di Marco, Gianluca Memoli, and Akio Tomiyama. Measurements of rising velocity of a small bubble in a stagnant fluid in one- and two-component systems. *Experimental Thermal and Fluid Science*, 31(6):609 – 623, 2007.

[5]D. Rabaud, P. Thibault, J. Raven, O. Hugon, E. Lacot, and P. Marmottant. Manipulation of confined bubbles in a thin microchannel: Drag and acoustic bjerknes forces. *Physics of Fluids*, 23:042003, 2011.

[6]R. Clift, J. R. Grace, and M. E. Weber. *Bubbles, drops and particles*. Academic Press, 1978.

[7]Rune Barnkob, Per Augustsson, Thomas Laurell, and Henrik Bruus. Acoustic radiation- and streaming-induced microparticle velocities determined by microparticle image velocimetry in an ultrasound symmetry plane. *Phys. Rev. E*, 86:056307, Nov 2012.

[8]T.G. Leighton. The inertial terms in equations of motion for bubbles in tubular vessels or between plates. *The Journal of the Acoustical Society of America*, 130(5):3333–3338, 2011.

[9]E.(Editor) Barsoukov and J.(Editor) Ross Macdonald. *Impedance spectroscopy: Theory, Experiment, and Applications*. New Jersey, Wiley-Blackwell, 2005.